JACS
JOURNAL OF THE AMERICAN CHEMICAL SOCIETY

ARTICLE

pubs.acs.org/JACS

Influence of H-Bond Strength on Chelate Cooperativity

Christopher A. Hunter,* Maria Cristina Misuraca, and Simon M. Turega

Department of Chemistry, University of Sheffield, Sheffield S3 7HF, United Kingdom

Supporting Information

ABSTRACT: Intermolecular complexes formed between metalloporphyrins and pyridine ligands equipped with multiple H-bond donors and acceptors have been used to measure the free energy contributions due to intramolecular ether−phenol H-bonding in the 24 different supramolecular architectures using chemical double mutant cycles in toluene. The ether−phenol interactions are relatively weak, and there are significant populations of partially bound states where between zero and four intramolecular H-bonds are made in addition to the porphyrin−ligand coordination interaction. The complexes were analyzed as ensembles of partially bound states to determine the effective molarities for the intramolecular interactions by comparison with the corresponding intermolecular ether−phenol H-bonds. The properties of the ether−phenol interactions were compared with phosphonate diester−phenol interactions in a closely related ligand system, which has more powerful H-bond acceptor oxygens positioned at the same location on the ligand framework. This provides a comparison of the properties of weak and strong H-bonds embedded in the same 24 supramolecular architectures. When the product of the intermolecular association constant and the effective molarity *KEM* > 1, there is a linear increase in the free energy contribution due to H-bonding with log *EM*, because the intramolecular interactions contribute fully to the stability of the complex. When *KEM* < 1, the H-bonded state is not significantly populated, and there is no impact on the overall stability of the complex. Intermolecular phosphonate diester−phenol H-bonds are 2 orders of magnitude stronger than ether−phenol H-bonds in toluene, so for the phosphonate diester ligand system, 23 of the 24 supramolecular architectures make intramolecular H-bonds. However, only 8 of these architectures lead to detectable H-bonding in the ether ligand system. The other 15 complexes have a suitable geometry for formation of H-bonds, but the ether−phenol interaction is not strong enough to overcome the reorganization costs associated with making intramolecular contacts, i.e., *KEM* < 1 for the ether ligands, and *KEM* > 1 for the phosphonate diester ligands. The values of *EM* measured for two different types of H-bond acceptor are linearly correlated, which suggests that *EM* is a property of the supramolecular acrchitecture. However, the absolute value of *EM* for an intramolecular phosphonate diester H-bond is about 4 times lower than the corresponding value for an intramolecular ether−phenol interaction embedded in the same supramolecular framework, which suggests that there may be some interplay of *K* and *EM*.

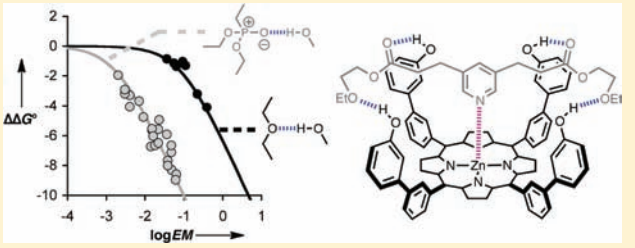

INTRODUCTION

Cooperativity is a phenomenon that we understand very well at a qualitative level, but rather poorly at a quantitative level.[1−6] Almost all functional molecular systems in biology, materials, and nanotechnology involve multiple cooperative intermolecular interactions between macromolecular surfaces.[7−18] Many factors contribute to the thermodynamic properties of these interfaces: electrostatic interactions between charges, H-bonds, aromatic interactions, desolvation, changes in conformation, etc. This complexity makes it difficult to disentangle the relative contributions of individual interactions, so new experiments are required if we are to develop a quantitative understanding of cooperativity that can be used in molecular design.[19−29]

Here we focus on chelate cooperativity, which is observed as an increase in binding affinity due to intramolecular interactions. Chelate cooperativity is quantified using the effective molarity for the intramolecular interaction, *EM*. The value of *EM* is expected to decrease with restriction of conformational flexibility or with conformational strain in the bound state,[30,31] but the magnitude of these effects is difficult to predict *a priori*, and so we have adopted an experimental approach. Synthetic supramolecular systems provide a controlled environment for systematic exploration of the factors that have an effect on cooperative binding.[32−35] We have studied the effect of the number of H-bonds on chelate cooperativity and demonstrated that when relatively rigid molecules are involved, the thermodynamic properties of a multivalent system are an additive function of the free energy contributions of the individual interactions. We have also investigated the role played by conformational flexibility in formation of intramolecular H-bonds. Preorganization of the interacting partners increases the stability of a complex, but the effects are not dramatic, because *EM* is a logarithmic function of the number of rotors linking the binding sites.[36,37]

Metalloporphyrin−ligand complexes of the type shown in Figure 1 provide an ideal platform for systematic studies of the relationship between supramolecular architecture and effective molarity in a relatively complicated but tractable molecular

Received: September 3, 2011
Published: November 23, 2011

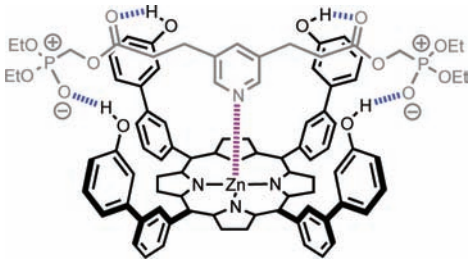

Figure 1. Structure of a complex formed between a zinc porphyrin (black) and a pyridine ligand (gray), which forms four intramolecular H-bonds (blue).

recognition interface. We have previously shown how chemical double mutant cycles (DMC) can be used to dissect the free energy contributions of individual functional group interactions to the overall stability of the complex. The strengths of intramolecular phosphonate diester−phenol H-bonds were measured for 24 different supramolecular architectures by using a set of closely related receptors and ligands with varying degrees of geometrical complementarity and conformational flexibility.

In this paper, we report the effect of changing the H-bonding properties of the functional groups on the cooperative properties of the system. Specifically, the phosphonate diester groups on the ligands have been exchanged for ethers, ensuring that the H-bond acceptor oxygens involved in formation of intramolecular interactions are located at identical positions on the ligand framework (Figure 2). Ethers are much weaker H-bond acceptors than phosphonate diesters, and although the phosphonate diester to ether mutation does introduce subtle changes in the conformational properties of the linker, e.g., the P−O bond is longer than the C−O bond, the geometries are similar. Thus, the ether ligand system significantly alters the properties of the individual H-bonding interactions without a significant change in supramolecular architecture. Comparison of the behavior of the two different ligand systems in the same 24 supramolecular architectures provides new insight into the nature of the relationship between the properties of individual functional group interactions and the manifestation of chelate cooperativity.

APPROACH

Figure 3a illustrates the chemical double mutant cycle (DMC) that is used to measure the free energy contribution of an intramolecular H-bond between two functional groups, **A** and **D**, to the stability of a complex that is held together by a stronger porphyrin−ligand coordination bond, **P•L**. The DMC is a generic tool for dissecting the contribution of individual intermolecular interactions to the overall stability of a multidentate complex, because it removes substituent effects as well as the secondary interactions that are highlighted in Figure 3a.[2,38] The single mutant arms of the DMC, B→D and C→D, quantify the magnitudes of secondary interactions, so that eq 1 provides a direct measurement of the free energy contribution of the **A•D** interaction to the overall stability of complex A.[2,39]

$$\Delta\Delta G^\circ = \Delta G^\circ_A - \Delta G^\circ_B - \Delta G^\circ_C + \Delta G^\circ_D \quad (1)$$

The formation of a cooperative molecular recognition interface can be formulated as a stepwise process, where the first

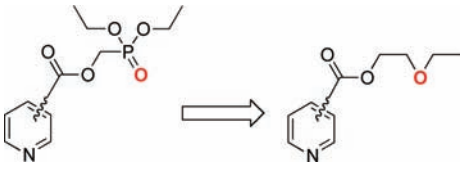

Figure 2. Phosphonate diester ligands have been exchanged for ether ligands, which have the key H-bond acceptor group (red) at the same location on the ligand framework.

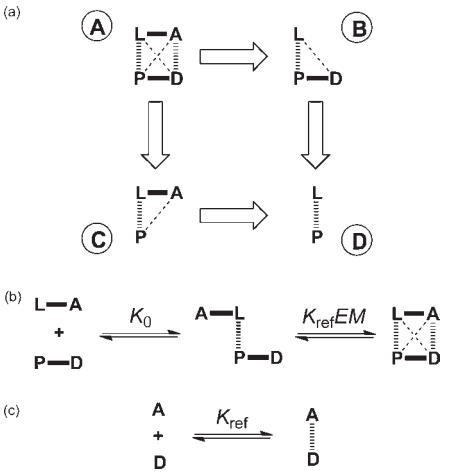

Figure 3. (a) Chemical double mutant cycle (DMC) used to measure the free energy contribution of the intramolecular **A•D** H-bond to the overall stability of complex A, which also contains a porphyrin−ligand coordination interaction (**P•L**). The contributions of secondary interactions (---) to the **A•D** interaction are removed by the DMC. (b) Stepwise representation of the assembly of complex A considered as formation of the strong intermolecular **P•L** coordination interaction followed by the weaker intramolecular **A•D** H-bond. K_0 is the intermolecular binding constant associated with the metal−ligand interaction, the product $K_{ref}EM$ is the equilibrium constant for formation of the intramolecular H-bond, K_{ref} is the equilibrium constant for formation of the corresponding intermolecular H-bond, and *EM* is the effective molarity for the intramolecular interaction. If $K_{ref}EM < 1$, the partially bound intermediate that lacks the H-bond is highly populated in the bound state. (c) Monofunctional reference compounds are used to characterize the intermolecular **A•D** H-bond, K_{ref}.

interaction is intermolecular and subsequent interactions are intramolecular (Figure 3b). The intramolecular equilibrium constant is conventionally expressed as the product of an intermolecular association constant, K_{ref}, and an effective molarity, *EM*.[1] This separates the thermodynamic properties of chelate cooperativity into an interaction term, K_{ref}, which is related to the intrinsic strength of the functional group interaction, and a cooperativity term, *EM*, which is related to the supramolecular architecture of the system. There is an assumption that these two parameters are independent, and in this paper, we test this assumption. Comparison of the properties of the phosphonate diester ligand system with the corresponding ether ligands allows us to change the strength of the H-bond interaction without changing the supramolecular architecture. Experimentally, *EM* is determined using eq 2, which combines the value of $\Delta\Delta G^\circ$ measured in a DMC with the intermolecular association constant, K_{ref}, measured for a 1:1 complex formed between two reference compounds that can only form the

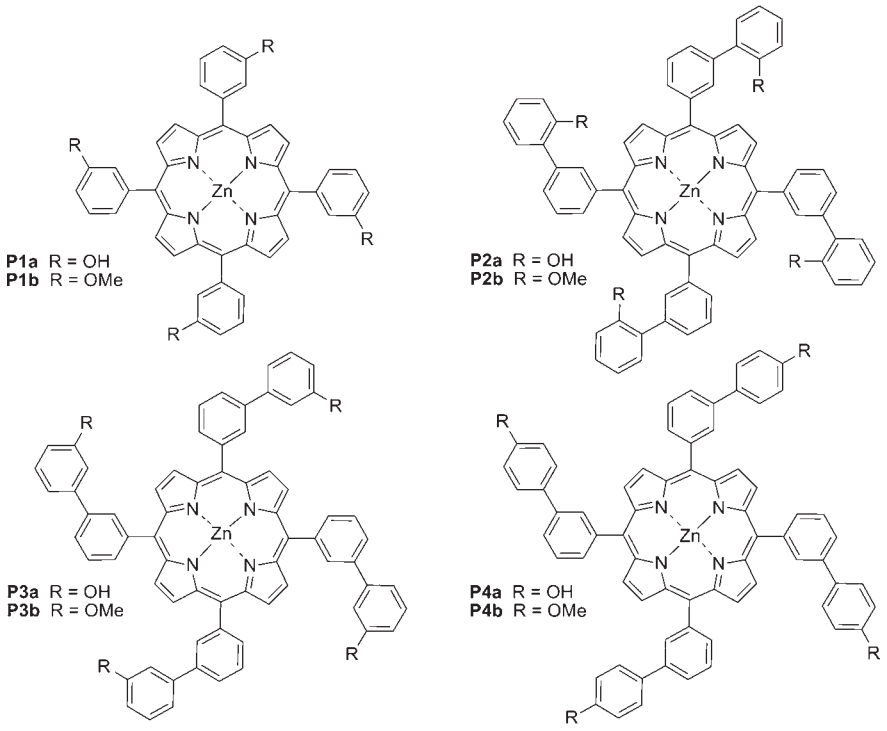

Figure 4. Porphyrin receptors, **P1a**–**P4a** (R = OH) and **P1b**–**P4b** (R = OMe).

A•D interaction (Figure 3c).

$$\Delta\Delta G^\circ = -RT \ln(1 + K_{ref}EM) \quad (2)$$

There are two terms inside the logarithm in eq 2, because there are two different bound states of the **LA•PD** complex. As illustrated in Figure 3b, there is one state in which the intramolecular H-bond is made, which has a stability constant $K_0K_{ref}EM$, and another in which there are no H-bonds, which has a stability constant K_0. Thus, the observed association constant for formation of the **LA•PD** complex is given by $K_0(1 + K_{ref}EM)$. For strong interactions like coordination bonds, $K_{ref}EM$ is usually large, and the equilibrium in Figure 3b lies to the right, so that the complex is fully assembled. However, for weak interactions like H-bonds, $K_{ref}EM$ can be close to or less than one, so that there is an equilibrium between fully and partially bound states. As we will show, treatment of the complex as an ensemble of different bound states is important for understanding the nature of cooperativity in multiply H-bonded complexes.

We have used this approach to explore the effect of supramolecular architecture, geometrical complementarity, and conformational flexibility on chelate cooperativity in the assembly of molecular recognition interfaces with up to five different intermolecular interactions.[39] Characterization of the complexes formed between 8 zinc porphyrins (Figure 4) and 15 pyridine ligands (Figure 5) in toluene allowed construction of 48 different DMCs. The metalloporphyrins have a rigid framework with four peripheral H-bonding sites and a central metal core.[4,40] The zinc–pyridine coordination bond provides a strong anchoring interaction promoting the cooperative formation of weaker intramolecular H-bonds between phenol H-bond donors on the porphyrin and carboxylate ester and phosphonate diester H-bond acceptors on the ligand. Measurement of intermolecular interactions with reference compounds indicates that phosphonate diester–phenol H-bonds (K_{ref} = 140 M^{-1}) are 2 orders of magnitude stronger than ester–phenol H-bonds (K_{ref} = 3 M^{-1}) in toluene, and as expected, the phosphonate diester interactions contribute significantly more to the stability of the porphyrin–ligand complexes (−6 to −9 kJ mol^{-1}) than H-bonds to the carboxylate esters (−3 kJ mol^{-1}). However, the corresponding values of *EM* for intramolecular ester–phenol H-bonds (200 mM) are on average an order of magnitude higher than those found for phosphonate diester–phenol H-bonds (30 mM). The ester and phosphonate diester groups are located at different positions on the ligand framework, which means that the *EM* values cannot be directly compared. In order to establish the effect of H-bond strength on chelate cooperativity, we designed ether analogues of the phosphonate diester ligands with H-bond acceptor groups located at identical positions on the ligand framework (compare ligands **La** and **Ld** in Figure 5, cf. Figure 2). Here we report the results of DMC experiments on the ether ligand system.

RESULTS

Synthesis. Synthesis of the eight porphyrins used in this work has been published previously.[39] Some of the ligands, ethyl isonicotinate (**L1b**), ethyl nicotinate (**L2b**), 4-picoline (**L4c**), 3-picoline (**L5c**), and 3,5-lutidine (**L6c**), were commercially available, and they were used directly without further purification. Ligands **L1d**–**L6d** were synthesized from the corresponding carboxylic acids (see Supporting Information).

UV–Vis Titration Experiments. Binding of the ligands to the porphyrins was investigated in toluene using UV–vis absorption spectroscopy and an automated titration experiment described previously.[39] The red shift observed in the Soret band of the porphyrin is a signature of metal–pyridine coordination, and this change was used to determine the association constants of the complexes. The titration data fit well to a 1:1 binding isotherm in

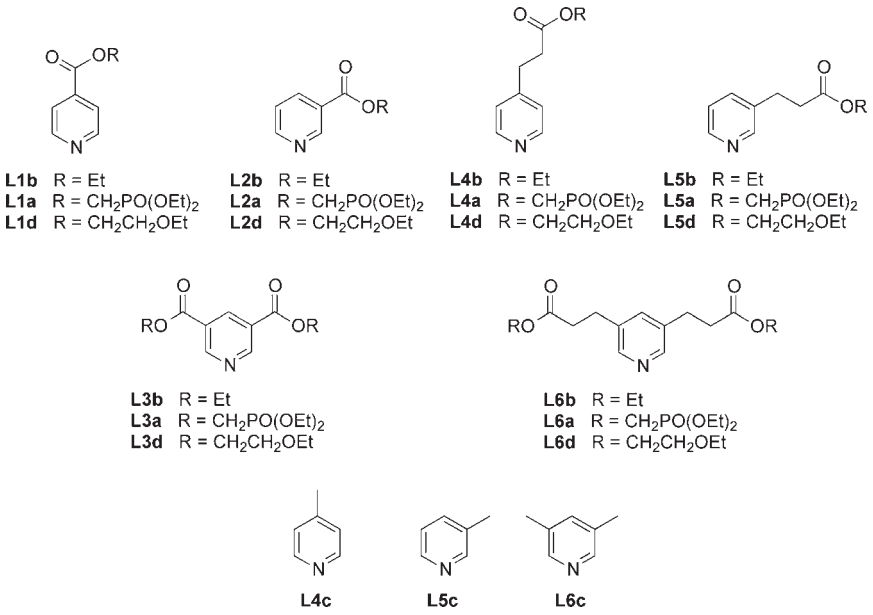

Figure 5. Pyridine ligands used to measure phosphonate diester−phenol H-bonds (**La**) and ether−phenol H-bonds (**Ld**). Ligands **Lb** quantify contributions from ester−phenol H-bonds, and ligands **Lc** quantify changes in the pyridine−zinc interactions in DMCs.

Table 1. Association Constants (K_{obs}/M^{-1}) for the Formation of 1:1 Complexes in Toluene at 298 K[a]

	porphyrin							
ligand	**P1a**	**P2a**	**P3a**	**P4a**	**P1b**	**P2b**	**P3b**	**P4b**
L1b	2.6×10^3 (10%)	4.2×10^3 (20%)	7.3×10^3 (30%)	3.5×10^3 (4%)	3.4×10^3 (20%)	3.0×10^3 (20%)	4.6×10^3 (40%)	3.9×10^3 (20%)
L2b	3.5×10^3 (20%)	4.9×10^3 (20%)	7.5×10^3 (20%)	5.1×10^3 (20%)	3.7×10^3 (30%)	3.2×10^3 (30%)	5.0×10^3 (7%)	5.2×10^3 (20%)
L3b	3.0×10^3 (20%)	4.0×10^3 (40%)	6.9×10^3 (9%)	5.1×10^3 (40%)	3.8×10^3 (20%)	2.6×10^3 (10%)	6.0×10^3 (20%)	4.5×10^3 (10%)
L4b	1.5×10^4 (20%)	2.0×10^4 (20%)	3.9×10^4 (30%)	2.5×10^4 (8%)	1.3×10^4 (10%)	1.1×10^4 (20%)	1.9×10^4 (20%)	1.6×10^4 (20%)
L5b	2.0×10^4 (40%)	3.1×10^4 (60%)	5.7×10^4 (40%)	1.3×10^4 (20%)	6.9×10^3 (30%)	5.2×10^3 (20%)	9.1×10^3 (30%)	8.8×10^3 (20%)
L6b	2.8×10^4 (20%)	4.9×10^4 (40%)	1.2×10^5 (30%)	7.5×10^3 (30%)	4.7×10^3 (30%)	2.8×10^3 (20%)	6.0×10^3 (20%)	5.3×10^3 (30%)
L4c	1.3×10^4 (7%)	1.8×10^4 (8%)	2.6×10^4 (6%)	2.1×10^4 (6%)	1.4×10^4 (10%)	1.1×10^4 (3%)	2.0×10^4 (7%)	1.8×10^4 (6%)
L5c	7.3×10^3 (6%)	1.0×10^4 (4%)	1.3×10^4 (2%)	1.1×10^4 (1%)	7.6×10^3 (20%)	6.8×10^3 (5%)	1.2×10^4 (2%)	1.0×10^4 (3%)
L6c	7.9×10^3 (20%)	1.2×10^4 (9%)	1.7×10^4 (6%)	1.4×10^4 (2%)	1.1×10^4 (3%)	8.2×10^3 (2%)	1.6×10^4 (6%)	1.3×10^4 (4%)
L1d	2.3×10^3 (9%)	3.3×10^3 (3%)	6.4×10^3 (20%)	3.1×10^3 (10%)	3.3×10^3 (20%)	2.4×10^3 (3%)	4.8×10^3 (20%)	3.1×10^3 (20%)
L2d	1.1×10^4 (8%)	5.3×10^3 (4%)	1.3×10^4 (4%)	6.0×10^3 (3%)	3.2×10^3 (1%)	2.5×10^3 (2%)	5.0×10^3 (1%)	3.8×10^3 (50%)
L3d	4.7×10^4 (2%)	4.3×10^3 (10%)	1.3×10^4 (8%)	3.0×10^3 (6%)	2.2×10^3 (10%)	1.4×10^3 (10%)	3.8×10^3 (8%)	2.1×10^3 (10%)
L4d	1.8×10^4 (20%)	2.2×10^4 (5%)	4.7×10^4 (10%)	4.2×10^4 (10%)	1.4×10^4 (10%)	1.1×10^4 (7%)	2.0×10^4 (10%)	1.6×10^4 (6%)
L5d	2.3×10^4 (20%)	3.3×10^4 (6%)	5.8×10^4 (2%)	1.5×10^4 (10%)	6.4×10^3 (10%)	4.3×10^3 (9%)	8.7×10^3 (5%)	7.4×10^3 (7%)
L6d	9.1×10^4 (10%)	1.6×10^5 (6%)	3.6×10^5 (6%)	2.0×10^4 (20%)	5.4×10^3 (2%)	3.8×10^3 (1%)	7.7×10^3 (10%)	5.7×10^3 (20%)

[a] Each titration was repeated at least three times, and the average values are reported with errors at the 95% confidence limit (percentage error reported in brackets).

all cases, and Table 1 shows the results. The association constants for the **Lb** and **Lc** ligands have been reported previously, but these experiments were repeated for internal consistency, and the results are practically identical to previous measurements.[39] The association constants span 2 orders of magnitude, 10^3-10^5 M^{-1}, and the data are illustrated graphically in Figure 6. The variation in stability is due to differences in the number, type, and geometry of H-bond interactions. The complexes formed between ligands bearing ether H-bond acceptors and porphyrins bearing H-bond donors (blue region) are in general more stable than the complexes where no intramolecular H-bonds can be made. Substituent effects can be observed for the metal−ligand interaction. When the ester moiety is linked directly to the pyridine ring, the electron-withdrawing effect of the carbonyl group makes the interaction between the nitrogen and the zinc weaker. The effect is more pronounced in the case of 4-substituted pyridine ligands, with differences of an order of magnitude in the metal−ligand interaction. The binding constants for the control complexes (green, yellow, and red in Figure 6) are generally lower, but some of the yellow complexes (complex B in the DMC) show enhanced stability due to interactions with the carboxylate ester H-bond acceptors on the ligands. Thus, more than one type of H-bond can be detected, and the contributions of multiple interactions have to be disentangled using DMCs.

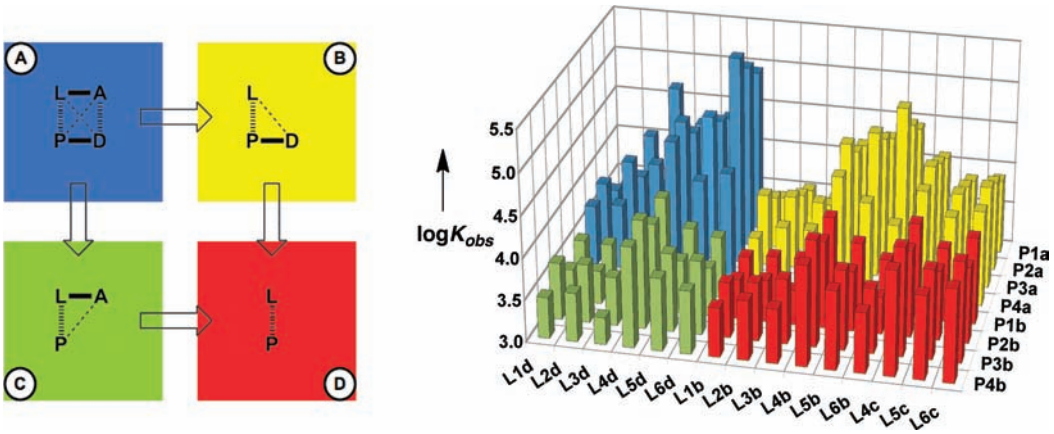

Figure 6. Association constants for the formation of the 1:1 complexes in toluene at 298 K (K_{obs}), color coded according to the DMC complexes, ether ligand−hydroxyporphyrin complexes in blue (**LA•PD**), ether ligand−methoxyporphyrin complexes in green (**LA•P**), and the control ligand−porphyrin complexes in yellow (**L•PD**) and in red (**L•P**).

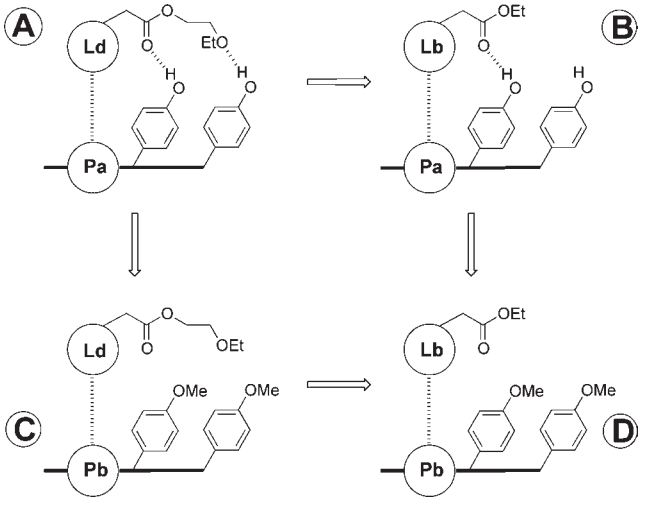

Figure 7. DMC for evaluating the thermodynamic contribution of ether−phenol H-bonds to the stability of complexes involving the **Ld** ligands.

DMC Analysis. Analysis of ester−phenol H-bonding in these complexes was reported previously, and details are provided in the Supporting Information.[39] The DMC in Figure 7 allows evaluation of the free energy contribution of ether−phenol H-bonds to the stability of a porphyrin−ligand complex in the presence of ester−phenol H-bonds. The overall stability of complex A in Figure 7 reflects contributions from the metal−ligand interaction, ester−phenol H-bonds, and secondary interactions, in addition to the ether−phenol H-bond. However, all of the other contributions are factored out by the DMC, allowing quantification of the ether−phenol interactions. For example, the ester−phenol H-bond appears both in complex A and in complex B, but not in complex C or in complex D, so the free energy contribution from this interaction cancels out in eq 1. There is an assumption in the DMC analysis that all free energy contributions are additive and formation of the ether−phenol H-bond does not affect the stability of the ester−phenol H-bond. The additive $\Delta\Delta G°$ increments observed when the properties of the one-armed ligand complexes are compared with those of the corresponding two-armed ligand complexes support this assumption.

Table 2. Free Energy Contributions from Ether−Phenol H-Bonds ($\Delta\Delta G°$/kJ mol^{-1}) to the Stability of Porphyrin−Ligand Complexes Determined in Toluene at 298 K Using the DMC in Figure 7[a]

	ligand					
porphyrin	L1d	L2d	L3d	L4d	L5d	L6d
P1a	0	-3	-8	0	-1	-3
P2a	0	-1	-2	0	-1	-2
P3a	0	-1	-3	0	0	-2
P4a	0	-1	-1	-1	-1	-2

[a] Average error over the data set ±1 kJ mol^{-1}. Entries where $\Delta\Delta G°$ is within the experimental error are shaded (cf. Figure 8).

The DMC results for ether−phenol H-bonds in the **Pa•Ld** complexes are reported in Table 2. Figure 8 illustrates possible geometries of the complexes. For the complexes where the H-bonding partners cannot get close to each other without distortion of the metal−ligand or the ether−phenol interaction, no ether−phenol H-bonding is observed, e.g., the **L1d** and **L4d** complexes. However, for complexes where the phenol and the ether groups can achieve close proximity, an intramolecular H-bond is detected by the DMC. For the two-armed ligands, **L3d** and **L6d**, the free energy contributions due to ether−phenol H-bonds are approximately double the $\Delta\Delta G°$ values for the corresponding one-armed ligands, **L2d** and **L5d**. In most of the one-armed ligand complexes, the value of $\Delta\Delta G°$ is zero within experimental error, so the free energy contributions due to these H-bonds can only be unambiguously measured in the two-armed ligand systems. It appears that one of the supramolecular architectures has an optimal geometry for formation of ether−phenol H-bonds, **P1a•L2d/L3d**. For these two complexes, each ether−phenol H-bond contributes −3 to −4 kJ mol^{-1} to the overall stability of the complex, which is similar to the result obtained for ester−phenol H-bonds.

Effective Molarities. In order to determine the values of *EM* for the intramolecular H-bonding interactions in these systems, reference compounds are required to measure K_{ref}, the association constant for formation of the corresponding intermolecular

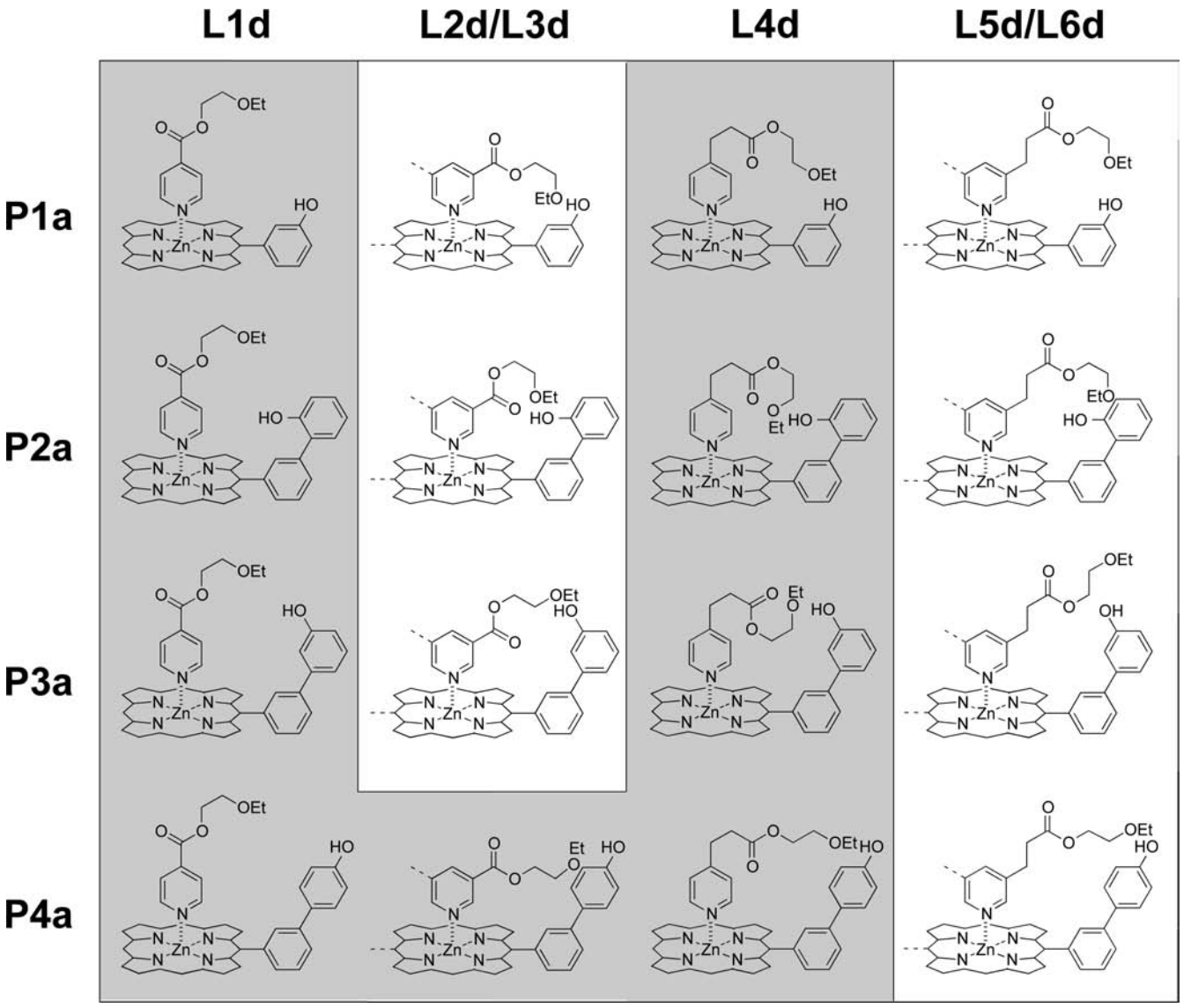

Figure 8. Illustration of possible geometries of complexes formed between **P1a**−**P4a** and **L1d**−**L6d**. Complexes where intramolecular ether−phenol H-bonds were not detected are shaded.

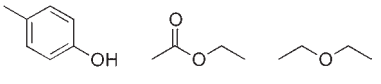

7 **8** **9**

Figure 9. Reference compounds used to measure intermolecular H-bond interactions.

H-bond (Figure 3). Figure 9 shows the structures of the monofunctional compounds that were used in ^{1}H NMR titrations to measure K_{ref} in toluene, and the results are listed in Table 3. The values for both the ester−phenol and the ether−phenol complexes are at the limit of reliable experimental measurement, but they are both in good agreement with the association constants estimated using eq 3, K_{calc}.[42]

$$-RT \ln K_{calc} = -(\alpha - \alpha_S)(\beta - \beta_S) + 6\ \text{kJmol}^{-1} \quad (3)$$

Table 3. Association Constants for the Formation of H-Bonded Complexes Measured in Toluene-d_8 at 298 K by ^{1}H NMR Titrations, K_{ref}, and Estimated Using Equation 3, K_{calc}[a]

complex	α	β	αs	βs	K_{ref}/M^{-1}	K_{calc}/M^{-1}
7•8	3.8	5.3	1.0	2.2	3 ± 1	3
7•9	3.8	5.3	1.0	2.2	3 ± 1	3

[a] H-bond parameters, α and β, from ref 42.

When a supramolecular system is held together by multiple weak H-bonds, the fully bound state, where all of the H-bonds are made simultaneously, is in equilibrium with all possible partially bound intermediates (cf. Figure 3b). The populations of these species depend on the products, K_iEM_i, the equilibrium constants for formation of intramolecular interactions. In general, for complexes that make N intramolecular H-bonds, the observed association constant, K_{obs}, is given by the sum of the equilibrium

Table 4. Effective Molarity (*EM*/mM) Values for Intramolecular Ether−Phenol H-Bonds Measured in Toluene at 298 K[a]

	ligand					
porphyrin	L1d	L2d	L3d	L4d	L5d	L6d
P1a	-[b]	220	410	-[b]	-[b]	110
P2a	-[b]	-[b]	36	-[b]	-[b]	92
P3a	-[b]	-[b]	66	-[b]	-[b]	93
P4a	-[b]	-[b]	-[b]	-[b]	-[b]	55

[a] Average error over the data set ±50%. [b] No H-bonding interaction detected.

constants for all of the bound states (eqs 4 and 5)

$$K_{obs} = fK_0 \tag{4}$$

where

$$f = 1 + \sum_i \sigma_i K_i EM_i + \sum_{i,j}^{N} \sigma_{ij} K_i EM_i K_j EM_j + \ldots + \sigma_{ij\ldots N} \prod_i^N K_i EM_i \tag{5}$$

and K_0 is the intermolecular association constant for formation of the zinc−nitrogen interaction, K_i is the association constant for formation of the corresponding intermolecular H-bond, EM_i is the effective molarity for formation of the intramolecular interaction, and σ are the statistical factors that account for the degeneracies of the partially bound states.

The contribution of the zinc−nitrogen interaction varies from one complex to another; i.e., K_0 is not a constant. However, differences in the zinc−nitrogen interaction cancel out in the DMC, so the value of $\Delta\Delta G^\circ$ measured in these experiments is related to the effective molarities in eq 5 by eq 6

$$e^{-\Delta\Delta G^\circ/RT} = \frac{f_A f_D}{f_B f_C} \tag{6}$$

where f_A−f_D are defined by eq 5 for the relevant complexes A−D in the DMC.

The experimental values of K_{ref} from Table 3 were used as K_i in eq 5, and the experimental values of $\Delta\Delta G^\circ$ from Table 2 were used in eq 6 to solve for the effective molarities of the intramolecular interactions, EM_i. Table 4 shows the results for the intramolecular ether−phenol H-bonds (see Supporting Information for the partially bound states analysis used to obtain the relationships for f_A−f_D in eq 5 and the corresponding results for the ester−phenol H-bonds). The highest value of *EM* measured for an intramolecular ether−phenol interaction is 410 mM. When there is a geometrical mismatch, the *EM* drops by up to an order of magnitude. The lower limit of detection is defined by the cases where H-bonding was too weak to be observed in the one-armed ligand complexes and could only be measured in the two-armed ligand complexes. The values of K_iEM_i are less than one in most cases, which means that the fully bound state is never highly populated and the partially bound intermediates predominate in these systems.

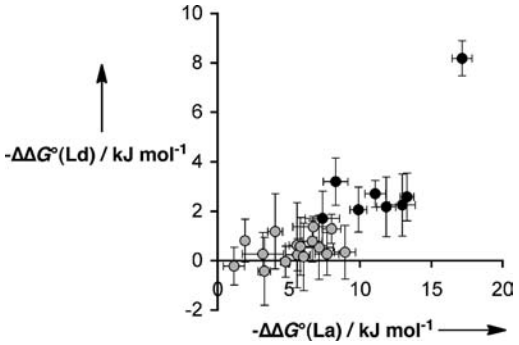

Figure 10. Free energy contributions due to intramolecular ether−phenol H-bonds, $\Delta\Delta G^\circ$(Ld), compared with the corresponding values for intramolecular phosphonate diester−phenol H-bonds, $\Delta\Delta G^\circ$(La), on the same ligand framework in toluene at 298 K. The black circles correspond to complexes that make detectable ether−phenol H-bonds, and the gray circles are complexes where $\Delta\Delta G^\circ$(Ld) is within error of zero.

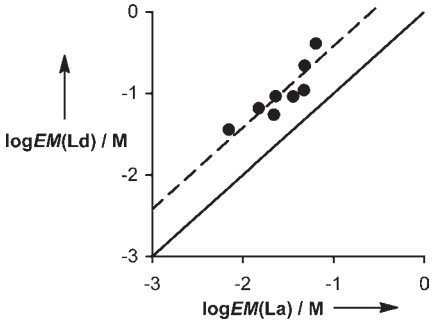

Figure 11. Effective molarities measured for intramolecular ether−phenol H-bonds, *EM*(Ld) from Table 4, compared with the corresponding values for intramolecular phosphonate diester−phenol H-bonds, *EM*(La) from ref 39, on the same ligand framework in toluene at 298 K. The solid line corresponds to $y = x$, and the dashed line corresponds to $y = x + 0.6$.

DISCUSSION

The properties of the complexes that contain intramolecular ether−phenol H-bonds can now be compared with the analogous complexes containing phosphonate diester groups.[39] The H-bond acceptor sites have the same position on the ligand framework in these two systems (Figure 2), and this provides us with an opportunity to compare the thermodynamic properties of weak and strong intramolecular H-bonds in the same supramolecular architecture. Figure 10 compares the DMC $\Delta\Delta G^\circ$ values for formation of intramolecular ether−phenol H-bonds, $\Delta\Delta G^\circ$(Ld), with the corresponding values measured for phosphonate diester−phenol H-bonds, $\Delta\Delta G^\circ$(La). The intramolecular phosphonate diester H-bonds are significantly stronger than the corresponding ether H-bonds in all cases. The intermolecular phosphonate diester−phenol association constant (K_{ref} = 140 M^{-1}) is 2 orders of magnitude larger than the ether−phenol interaction (K_{ref} = 3 M^{-1}), so this result is not surprising. Of the 24 different supramolecular architectures shown in Figure 8, only 8 give rise to detectable H-bonding interactions for the ether system, whereas phosphonate diester−phenol H-bonding was measurable in 23 of the complexes. While a clear trend is difficult to discern in Figure 10, the 8 complexes that make detectable ether−phenol H-bonds correspond to the architectures that make the strongest H-bonds in the

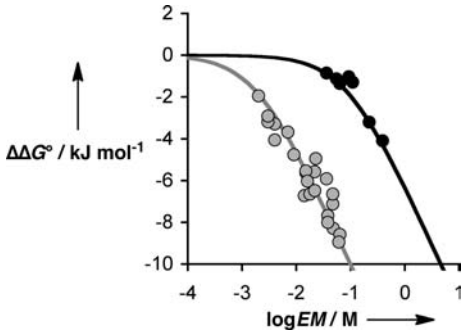

Figure 12. Relationship between the free energy contribution due an intramolecular interaction ($\Delta\Delta G^\circ$) and the effective molarity (EM) in toluene at 298 K. Experimental values for phosphonate diester−phenol H-bonds (gray circles) and ether−phenol H-bonds (black circles). The lines correspond to $\Delta\Delta G^\circ = -RT\ln(1 + 4K_{ref}EM)$, where the statistical factor of 4 is an estimate of the average statistical factor, σ, due to the presence of four H-bond donors on the porphyrins.

phosphonate diester system (black points in Figure 10). In both ligand systems, the **P1•L3** architecture leads to the strongest intramolecular H-bonding interactions, which is indicative of good geometric complementarity in these complexes. However, the effects are much more dramatic in the ether system, making the **P1a•L3d** complex a clear outlier in Figure 10.

Figure 11 compares the values of EM measured for intramolecular ether−phenol H-bonds in Table 4, EM(Ld), with the corresponding values for the phosphonate diester system, EM(La). The limiting value of K_iEM_i that leads to a measurable value of $\Delta\Delta G^\circ$ (<-1 kJ mol^{-1}) depends on the degeneracy of the complex but is of the order 0.1. For ether−phenol H-bonds, this places a lower limit of 30 mM on the measurable EM. The lower limit on EM for the phosphonate diester system is 0.7 mM. Thus, there are 15 supramolecular architectures where intramolecular H-bonding is not observed for the ether system, but in the phosphonate diester system, the H-bond interactions are strong enough to make intramolecular contacts even when there is significant geometrical strain.

There is a good correlation between the EM values measured for the two different ligand systems in Figure 11, and the slope of the best fit straight line is 0.9. Thus, the supramolecular architecture that has the highest EM and leads to the strongest phosphonate diester H-bonds, **P1•L3**, also gives the strongest ether H-bonds. It appears that differences in EM are transferable between different ligand systems, but the absolute values are not. The correlation in Figure 11 does not pass through the origin, and the values of EM for the phosphonate diester system are consistently smaller than those measured for the ether system by a factor of between 2 and 6.

The difference between the phosphonate diester and ether EM values could be due to a systematic error in the experiment. One potential source of systematic errors is the value of K_{ref}. The intermolecular association constant for the ether−phenol H-bond is small and difficult to measure accurately. However, K_{ref} would have to be 4 times bigger to account for the differences in Figure 11, and an association constant of 12 M^{-1} is straightforward to determine accurately. Similarly, the value of K_{ref} for the phosphonate diester interaction is too high (140 M^{-1}) to be subject to an error of this magnitude. Some of the factors that we have ignored may contribute to differences in EM: the phosphonate diester groups are bulkier than the ethers, the conformational flexibility of the ligand side-arms differ, solvation of the complexes depends on the details of the local structure, and the C−O and P−O bond lengths are different. The effects of solvation are likely to be specific to certain supramolecular architectures, but steric interactions or poor geometric complementarity might account for the smaller EMs observed for the phosphonate diester ligands. Another possibility is that strong H-bonding interactions impose constraints on the geometry of the complex, whereas weaker interactions lead to looser binding and residual conformational flexibility with a correspondingly larger EM. In other words, changes in K_{ref} may be partially compensated by changes in EM, so that these two parameters are not mutually independent. Further experiments on a wider range of functional group interactions will be required to test this hypothesis.

CONCLUSIONS

The metalloporphyrin−ligand system provides an ideal platform for conducting a systematic survey of the relationship between chemical structure and cooperativity at relatively complex molecular recognition interfaces. An automated UV−vis titration system has been employed to characterize different metalloporphyrin−ligand combinations. In order to factor out the thermodynamic contributions of individual interactions, we have developed an approach based on chemical double mutant cycles. The titration data have been used to construct DMCs to examine a variety of closely related intramolecular H-bonds in different supramolecular architectures. The free energy contributions of individual functional group interactions have been characterized in terms of effective molarities for the intramolecular processes.

The experiments described here allow us to make a direct comparison of the properties of two different functional group interactions embedded in 24 different supramolecular architectures. Intermolecular phosphonate diester−phenol H-bonds are 2 orders of magnitude stronger than ether−phenol H-bonds in toluene, and this difference is reflected in the properties of the intramolecular interactions measured in the porphyrin−ligand complexes. Figure 12 illustrates the relationship between the effective molarity, EM, and the resulting free energy contribution to the overall stability of a supramolecular complex, $\Delta\Delta G^\circ$. When $K_{ref}EM > 1$, there is a linear increase in $\Delta\Delta G^\circ$ with log EM, because the intramolecular interactions contribute fully to the stability of the complex. However when $K_{ref}EM < 1$, the H-bonded state is not significantly populated, and $\Delta\Delta G^\circ$ tends to zero. Thus, there is a lower limit in the value of EM, below which intramolecular H-bonding does not affect the overall stability of a complex. However, the value of this lower limit in EM depends on the strength of the functional group interaction, i.e., K_{ref}. Experiments on the phosphonate diester ligand system show that there are 23 different supramolecular architectures that are compatible with the formation of intramolecular H-bonds (gray data in Figure 12). However, only 8 of these architectures lead to detectable H-bonding in the ether ligand system (black data in Figure 12). The other 15 complexes have a suitable geometry for formation of H-bonds, but the ether−phenol interaction is not strong enough to overcome the reorganization costs associated with making intramolecular contacts.

The values of EM measured for two different types of H-bond acceptor located at the same positions on the ligand framework are linearly correlated, which suggests that EM is a property of the supramolecular architecture. However, the interplay of EM and K_{ref} means that expression of chelate cooperativity is a function of both the supramolecular architecture and the properties of the interaction. For example, the large free energy contribution due

to ether−phenol H-bonding in the **P1a•L3d** complex appears to be anomalous in Figure 10. However, the values of *EM* for the corresponding phosphonate diester system show that the **P1•L3** architecture has the best geometry for formation of intramolecular H-bonds. For **P1a•L3d**, the increased *EM* pushes the product $K_{ref}EM$ over the threshold required for intramolecular H-bonds to contribute fully to the stability of the complex. Thus, the anomaly stems from the fact that the **P1a•L3d** complex is the only ether ligand complex where $K_{ref}EM > 1$. For systems where $K_{ref}EM$ is close to one, subtle changes in conditions can lead to dramatic differences in the expression of cooperativity, because intramolecular interactions can effectively be turned on and off by relatively small changes in *EM* or K_{ref}. This is one of the hallmarks of cooperativity in biomolecules.

Although the values of *EM* for ether and phosphonate diester ligands are correlated, the absolute values differ. The value of *EM* for an intramolecular phosphonate diester H-bond is about 4 times lower than the corresponding value for an intramolecular ether−phenol interaction embedded in the same supramolecular framework. This observation suggests that the interplay of K_{ref} and *EM* may modulate the absolute value of *EM*, so that this parameter is not a truly independent property of the supramolecular architecture. One possibility is that stronger intramolecular interactions lead to lower *EM* values, because the complex is more highly organized. Alternatively, subtle differences in geometry or steric hindrance might make it more difficult to make intramolecular phosphonate diester interactions. This is the subject of current investigation in our laboratory using a wider variety of functional group interactions.

EXPERIMENTAL SECTION

UV−Vis Titration Experiments. A 10 mL sample of porphyrin dissolved in toluene was prepared at known concentration (3−13 μM). A 10 mL solution of ligand was prepared in toluene at known concentration (0.05−5.5 mM). A BMG FLUOstar Omega plate reader equipped with a UV−vis detector was employed. A 96-well Hellma quartz plate was loaded with a known volume of host solution (150 μL per well). Each experiment used 12 wells, so that one ligand solution could be titrated into four different porphyrin solutions in triplicate. Toluene is a high-boiling point liquid, and no solvent evaporation occurred on the time scale of the data acquisition. By using the internal injection pumps, small aliquots of the ligand solution (3, 6, and 10 μL) were successively added into the porphyrin solution, and the absorbance at five selected wavelengths was measured after each addition. Changes in the absorbance of the Soret band of the porphyrin were fit to a 1:1 binding isotherm using purpose written software. The error is quoted as twice the standard deviation.

^{1}H NMR Titrations. A 2-mL sample of host dissolved in toluene-d_8 was prepared at known concentration (7−270 mM). A 0.6 mL fraction of this solution was used to record a ^{1}H NMR spectrum. The host stock solution was used to prepare a 1 mL solution of guest at known concentration (70−2600 mM), so that the concentration of host remained constant throughout the titration. Aliquots of guest solution were successively added to the NMR tube containing the host solution, and a ^{1}H NMR spectrum was recorded after each addition. Changes in chemical shifts were fit to 1:1 binding isotherms using purpose written software. Each titration was repeated at least three times, and the error is quoted as twice the standard deviation.

ASSOCIATED CONTENT

Supporting Information. Synthetic procedures, spectroscopic data, analysis of the partially bound states, tables of *KEM* values and occupancies for intramolecular H-bonds. This material is available free of charge via the Internet at http://pubs.acs.org.

AUTHOR INFORMATION

Corresponding Author
c.hunter@sheffield.ac.uk

ACKNOWLEDGMENT

We thank the EPSRC for funding and Dr. M. Fisher for assistance with protocols for the BMG Labtech plate reader.

REFERENCES

(1) Hunter, C. A.; Anderson, H. L. *Angew. Chem., Int. Ed.* **2009**, *48*, 7488–7499.
(2) Camara-Campos, A.; Musumeci, D.; Hunter, C. A.; Turega, S. *J. Am. Chem. Soc.* **2009**, *131*, 18518–18524.
(3) Hunter, C. A.; Ihekwaba, N.; Misuraca, M. C.; Segarra-Maset, M. D.; Turega, S. M. *Chem. Commun.* **2009**, 3964–3966.
(4) Chekmeneva, E.; Hunter, C. A.; Packer, M. J.; Turega, S. M. *J. Am. Chem. Soc.* **2008**, *130*, 17718–17725.
(5) Schneider, H.-J. *Angew. Chem., Int. Ed.* **2009**, *48*, 3924–3977.
(6) Ercolani, G. *J. Am. Chem. Soc.* **2003**, *125*, 16097–16103.
(7) Gargano, J. M.; Ngo, T.; Kim, J. Y.; Acheson, D. W. K.; Lees, W. J. *J. Am. Chem. Soc.* **2001**, *123*, 12909–12910.
(8) Dam, T. K.; Roy, R.; Das, S. K.; Oscarson, S.; Brewer, C. F. *J. Biol. Chem.* **2000**, *275*, 14223–14230.
(9) Gestwick, J. E.; Strong, L. E.; Kiessling, L. L. *Chem. Biol.* **2000**, *7*, 583–591.
(10) Kitov, P. I.; Sadowska, J. M.; Mulvey, G.; Armstrong, G. D.; Ling, H.; Pannu, N. S.; Read, R. J.; Bundle, D. R. *Nature* **2000**, *403*, 669–672.
(11) Crothers, D. M.; Metzger, H. *Immunochemistry* **1972**, *9*, 341–357.
(12) Mulder, A.; Huskens, J.; Reinhoudt, D. N. *Org. Biomol. Chem.* **2004**, *2*, 3409–3424.
(13) Mammen, M.; Choi, S. K.; Whitesides, G. M. *Angew. Chem., Int. Ed.* **1998**, *37*, 2755–2794.
(14) Badjic, J. D.; Nelson, A.; Cantrill, S. J.; Turnbull, W. B.; Stoddart, J. F. *Acc. Chem. Res.* **2005**, *38*, 723–732.
(15) Philp, D.; Stoddart, J. F. *Angew. Chem., Int. Ed.* **1996**, *35*, 1155–1196.
(16) Anderson, H. L. *Inorg. Chem.* **1994**, *33*, 972–981.
(17) De Greef, T. F. A.; Smulders, M. M. J.; Wolffs, M.; Schenning, A. P. H. J.; Sijbesma, R. P.; Meijer, E. W. *Chem. Rev.* **2009**, *109*, 5687–5754.
(18) De Greef, T. F. A.; Nieuwenhuizen, M. M. L.; Sijbesma, R. P.; Meijer, E. W. *J. Org. Chem.* **2010**, *75*, 598–610.
(19) Jencks, W. P. *Proc. Natl. Acad. Sci. U.S.A.* **1981**, *78*, 4046–4050.
(20) Lehn, J.-M.; Rigault, A.; Siegel, J.; Harrowfield, J.; Chevrier, B.; Moras, D. *Proc. Natl. Acad. Sci. U.S.A.* **1987**, *84*, 2565–2569.
(21) Williams, D. H.; Maguire, A. J.; Tsuzuki, W.; Westwell, M. S. *Science* **1998**, *280*, 711–714.
(22) Calderone, C. T.; Williams, D. H. *J. Am. Chem. Soc.* **2001**, *123*, 6262–6267.
(23) Williams, D. H.; Davies, N. L.; Zerella, R.; Bardsley, B. *J. Am. Chem. Soc.* **2004**, *126*, 2042–2049.
(24) Huskens, J.; Mulder, A.; Auletta, T.; Nijhuis, C. A.; Ludden, M. J. W.; Reinhoudt, D. N. *J. Am. Chem. Soc.* **2004**, *126*, 6784–6797.
(25) Hunter, C. A.; Tomas, S. *Chem. Biol.* **2003**, *10*, 1023–1032.
(26) Tobey, S. L.; Anslyn, E. V. *J. Am. Chem. Soc.* **2003**, *125*, 10963–10970.
(27) Hughes, A. D.; Anslyn, E. V. *Proc. Natl. Acad. Sci. U.S.A.* **2007**, *104*, 6538–6543.

(28) Camara-Campos, A.; Hunter, C. A.; Tomas, S. *Proc. Natl. Acad. Sci. U.S.A.* **2006**, *103*, 3034–3038.
(29) Mati, I. K.; Cockroft, S. L. *Chem. Soc. Rev.* **2010**, *39*, 4195–4205.
(30) Chi, X. L.; Guerin, A. J.; Haycock, R. A.; Hunter, C. A.; Sarson, L. D. *Chem. Commun.* **1995**, 2563–2565.
(31) Krishnamurthy, V. M.; Semetey, V.; Bracher, P. J.; Shen, N.; Whitesides, G. M. *J. Am. Chem. Soc.* **2007**, *129*, 1312–1320.
(32) Shinkai, S.; Ikeda, M.; Sugasaki, A.; Takeuchi, M. *Acc. Chem. Res.* **2001**, *34*, 494–503.
(33) Bissantz, C.; Kuhn, B.; Stahl, M. *J. Med. Chem.* **2010**, *53*, 5061–5084.
(34) Scarso, A.; Shivanyuk, A.; Rebek, J. *J. Am. Chem. Soc.* **2003**, *125*, 13981–13983.
(35) Cockroft, S. L.; Hunter, C. A. *Chem. Commun.* **2009**, 3961–3963.
(36) Cram, D. J. *Angew. Chem., Int. Ed. Engl.* **1986**, *25*, 1039–1057.
(37) Cram, D. J. *Angew. Chem., Int. Ed. Engl.* **1988**, *27*, 1009–1020.
(38) Cockroft, S. L.; Hunter, C. A. *Chem. Soc. Rev.* **2007**, *36*, 172–188.
(39) Hunter, C. A.; Misuraca, M. C.; Turega, S. M. *J. Am. Chem. Soc.* **2011**, *133*, 582–594.
(40) Kim, H.-J.; Bampos, N.; Sanders, J. K. M. *J. Am. Chem. Soc.* **1999**, *121*, 8120–8121.
(41) Mor, M.; Rivara, S.; Lodola, A.; Plazzi, P. V.; Tarzia, G.; Duranti, A.; Tontini, A.; Piersanti, G.; Kathuria, S.; Piomelli, D. *J. Med. Chem.* **2004**, *47*, 4998–5008.
(42) Hunter, C. A. *Angew. Chem., Int. Ed.* **2004**, *43*, 5310–5324.